

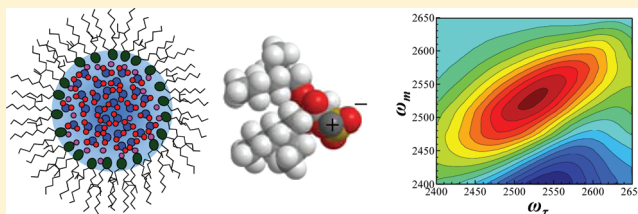
# Dynamics of Water at the Interface in Reverse Micelles: Measurements of Spectral Diffusion with Two-Dimensional Infrared Vibrational Echoes

Emily E. Fenn, Daryl B. Wong, Chiara H. Giammanco, and M. D. Fayer\*

Department of Chemistry, Stanford University, Stanford, California 94305, United States

**ABSTRACT:** Water dynamics inside of reverse micelles made from the surfactant Aerosol-OT (AOT) were investigated by observing spectral diffusion, orientational relaxation, and population relaxation using two-dimensional infrared (2D IR) vibrational echo spectroscopy and pump–probe experiments. The water pool sizes of the reverse micelles studied ranged in size from 5.8 to 1.7 nm in diameter. It is found that spectral diffusion, characterized by the frequency–frequency correlation function (FFCF), significantly changes as the water pool size decreases.

For the larger reverse micelles (diameter 4.6 nm and larger), the 2D IR signal is composed of two spectral components: a signal from bulk-like core water, and a signal from water at the headgroup interface. Each of these signals (core water and interfacial water) is associated with a distinct FFCF. The FFCF of the interfacial water layer can be obtained using a modified center line slope (CLS) method that has been recently developed. The interfacial FFCFs for large reverse micelles have a single exponential decay ( $\sim 1.6$  ps) to an offset plus a fast homogeneous component and are nearly identical for all large sizes. The observed  $\sim 1.6$  ps interfacial decay component is approximately the same as that found for bulk water and may reflect hydrogen bond rearrangement of bulk-like water molecules hydrogen bonded to the interfacial water molecules. The long time offset arises from dynamics that are too slow to be measured on the accessible experimental time scale. The influence of the chemical nature of the interface on spectral diffusion was explored by comparing data for water inside reverse micelles (5.8 nm water pool diameter) made from the surfactants AOT and Igepal CO-520. AOT has charged, sulfonate head groups, while Igepal CO-520 has neutral, hydroxyl head groups. It is found that spectral diffusion on the observable time scales is not overly sensitive to the chemical makeup of the interface. An intermediate-sized AOT reverse micelle (water pool diameter of 3.3 nm) is analyzed as a large reverse micelle because it has distinct core and interface regions, but its core region is more constrained than bulk water. The interfacial FFCF for this intermediate-sized reverse micelle is somewhat slower than those found for the larger reverse micelles. The water nanopools in the smaller reverse micelles cannot be separated into core and interface regions. In the small reverse micelles, the FFCFs are biexponential decays to an offset plus a fast homogeneous component. Each small reverse micelle exhibits an  $\sim 1$  ps decay time, which may arise from local hydrogen bond fluctuations and a slower,  $\sim 6$ –10 ps decay, which is possibly due to slow hydrogen bond rearrangement of noninterfacial water molecules or topography fluctuations at the interface.



## I. INTRODUCTION

The behavior and motions of interfacial water molecules are critical in many chemical reactions, biological mechanisms, and industrial processes. For example, water molecules facilitate proton transfer in the polyelectrolyte membranes of fuel cells. Water molecules at mineral or zeolite interfaces are used for ion-exchange and filtration applications as well as heterogeneous catalysis. In biology, water molecules are found in crowded environments interacting with protein pockets or surfaces, cell membranes, or pharmaceuticals. Processes in such nanoscopic systems depend upon water's ability to form and exchange hydrogen bonds. Bulk water consists of an extended network of hydrogen bonds that are continually rearranging, requiring concerted motions of both the first and second solvation shells.<sup>1,2</sup> The presence of interfaces or confined environments can disrupt pathways necessary for hydrogen bond rearrangement, thus slowing down the rate of hydrogen

bond exchange.<sup>3–7</sup> Spectroscopic observables that report upon water dynamics include the vibrational lifetime, orientational relaxation, and spectral diffusion of the water hydroxyl stretch, all of which generally occur on the picosecond (ps) time scale. With its femtosecond (fs) time resolution, ultrafast infrared spectroscopy is a useful technique for measuring water dynamics.

One fundamental question is how the size of the confining environment affects water hydrogen bond rearrangement dynamics. This topic has been explored quite extensively with ultrafast pump–probe experiments that measure water reorientation inside of reverse micelle systems.<sup>6,8–20</sup> A reverse micelle consists of a nanoscopic water pool surrounded by a layer of surfactant molecules. The surfactant has a hydrophilic headgroup

**Received:** July 19, 2011

**Revised:** September 3, 2011

**Published:** September 07, 2011

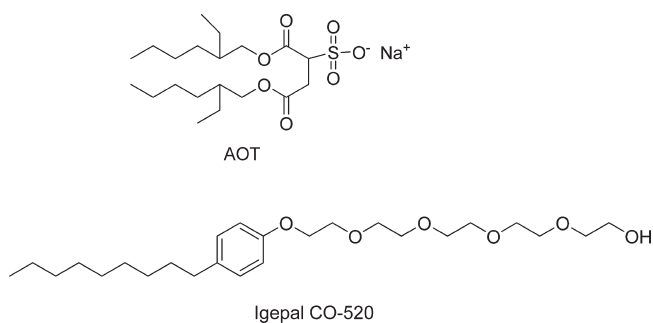


**Figure 1.** Molecular structures for AOT and Igepal CO-520. AOT has charged, sulfonate head groups, while Igepal has neutral, hydroxyl head groups.

and a hydrophobic tail region. The head groups face in toward the water pool, surrounding the nanoscopic pool of water and forming a layer of interfacial water molecules. The tails are suspended in a nonpolar organic phase. A common surfactant used in making reverse micelles is sodium bis(2-ethylhexyl) sulfosuccinate, also known as Aerosol-OT or AOT (Figure 1), which has charged, sulfonate head groups. The AOT system makes monodispersed, spherical reverse micelles and has been well-characterized. The size of the water pool diameter is easily controlled by varying the  $w_0$  parameter, which is equal to the ratio of concentrations of starting materials:  $w_0 = [\text{H}_2\text{O}]/[\text{surfactant}]$ .<sup>21–23</sup> Sizes of reverse micelles can range from essentially dry AOT ( $w_0 = 0$ ) all the way up to  $w_0 = 60$ , which has a water nanopool diameter of 28 nm and contains roughly 350 000 water molecules.<sup>10</sup>

Recently, the spectral diffusion dynamics of water inside of  $w_0 = 2$  AOT reverse micelles suspended in carbon tetrachloride ( $\text{CCl}_4$ ) were reported.<sup>24</sup> Spectral diffusion dynamics are described by the frequency–frequency correlation function (FFCF), which indicates how quickly water molecules sample different frequencies within the inhomogeneously broadened vibrational absorption band. The frequency evolution is caused by structural changes that influence the vibrational frequency of a molecule such as hydrogen bond rearrangement. Once the FFCF is known, time-dependent diagrammatic perturbation theory can be used to calculate all linear and nonlinear optical experimental observables.<sup>25</sup> In addition to a fast, homogeneous component, the FFCF for the  $w_0 = 2$  system was found to have  $\sim 1$  ps and  $\sim 10$  ps components and an offset.<sup>24</sup> The FFCF for bulk water has a homogeneous component, a  $\sim 400$  fs component, and a  $\sim 1.7$  ps component (and no offset).<sup>26</sup> The short ( $\sim 400$  fs) component is attributed to fast local hydrogen bond fluctuations, mainly in the lengths of hydrogen bonds,<sup>27,28</sup> while the 1.7 ps component arises from hydrogen bond network randomization.<sup>26</sup> While it is likely that the  $\sim 1$  ps component in the  $w_0 = 2$  system arises from fast hydrogen bond fluctuations, the 10 ps component has no analogue in the bulk water system. It was proposed that this  $\sim 10$  ps process was due to water molecules accommodating topography roughness of the surfactant interface, but other possibilities will be discussed below. The offset was attributed to extremely slow reorientation and diffusion processes of water molecules. Overall, the dynamics in the very small  $w_0 = 2$  reverse micelles ( $\sim 40$  water molecules) are extremely slow compared to bulk water because virtually all of the water molecules are interacting with the interface.

It was shown recently that the dynamics inside the AOT reverse micelles are insensitive to the identity of the nonpolar

phase.<sup>24</sup> AOT reverse micelles may be made in a variety of solvents, including isoctane, decane, carbon tetrachloride, and toluene, without significantly changing the size of the water pool.<sup>29,30</sup> Isooctane is a popular solvent used in experiments and in molecular dynamics (MD) simulations.<sup>31,32</sup> However, it was discovered that interactions between AOT and isoctane cause extra signals that interfere with the measurements of the hydroxyl stretch spectral diffusion, although it is still possible under the right circumstances to effectively background-subtract the extra signals and determine the FFCF.<sup>24</sup> This procedure that corrects for the distortions in the isoctane system has been described in detail.<sup>24</sup> When carbon tetrachloride ( $\text{CCl}_4$ ) is used as the solvent instead, the distortions are not present. To ascertain whether the identity of the nonpolar phase changes the dynamics of the water pool, the steady state and dynamic data were compared for AOT reverse micelles made in isoctane and in  $\text{CCl}_4$ . It was found that the Fourier transform infrared (FTIR) absorption spectra, vibrational lifetime behavior, reorientation dynamics, and spectral diffusion are identical for the two solvents within experimental error. Thus, experimental data obtained in  $\text{CCl}_4$  may be directly compared to experiments performed with isoctane.

Here, we compare the spectral diffusion dynamics of water inside a wide range of AOT reverse micelle sizes,  $w_0 = 16.5, 12, 7.5, 4$ , and  $2$ . However,  $\text{CCl}_4$  cannot support reverse micelles of  $w_0$ 's greater than  $10$ ,<sup>10,33</sup> so cyclohexane was used as the organic phase for  $w_0 = 12$  and  $16.5$ . On the basis of the previous solvent-dependence study, the change to cyclohexane will not affect the water pool dynamics. Spectral diffusion of water was also measured in reverse micelles of  $w_0 = 12$  made with the nonionic surfactant Igepal CO-520 (Figure 1), which has the same water pool diameter as AOT  $w_0 = 16.5$  (5.8 nm). With these different systems, we examine how both water pool size and the chemical composition of the interface affect water spectral diffusion, and therefore structural evolution, in confined environments.

## II. EXPERIMENTAL PROCEDURES

Carbon tetrachloride ( $\text{CCl}_4$ ), cyclohexane,  $\text{H}_2\text{O}$ ,  $\text{D}_2\text{O}$  (Sigma-Aldrich), and Igepal CO-520 were used as received. AOT (Sigma-Aldrich) was purified by first dissolving the compound in methanol and stirring overnight with activated charcoal. The charcoal was removed by vacuum filtration, and the methanol was removed with a rotary evaporator. The AOT was stored in a vacuum desiccator. Stock solutions (0.5 M) of AOT were prepared in  $\text{CCl}_4$  and in cyclohexane. A 0.3 M stock solution of Igepal CO-520 was prepared in cyclohexane. The residual water contents of the stock solutions were measured via Karl Fischer titration. The reverse micelle samples were prepared by mass by adding appropriate amounts of a solution of 5% HOD in  $\text{H}_2\text{O}$  to measured quantities of the AOT or Igepal stock solutions to obtain the desired  $w_0$ . The AOT/ $\text{CCl}_4$  stock solution was used to make  $w_0 = 2, 4$ , and  $7.5$  (diameters of 1.7, 2.3, and 3.3 nm, respectively), while the AOT/cyclohexane stock solution was used to make  $w_0 = 12$  and  $16.5$  (diameters of 4.6 and 5.8 nm, respectively). To compare the effects of the chemical composition of the interface, Igepal reverse micelles with  $w_0 = 12$  were also made. Like AOT, Igepal also makes monodispersed spherical reverse micelles.<sup>34</sup> The  $w_0 = 12$  Igepal reverse micelles have the same 5.8 nm diameter as AOT  $w_0 = 16.5$ . The  $w_0 = 12$  Igepal reverse micelles are not the same size as the  $w_0 = 12$  AOT reverse micelles because the two surfactants have

different aggregation numbers. The experimental samples are contained between two calcium fluoride windows that are separated by a Teflon spacer. The thickness of the Teflon spacer is chosen such that the optical density of the OD stretch region is  $\sim 0.1$  for the echo experiments.

In the ultrafast experiments, the OD stretch of 5% HOD in  $\text{H}_2\text{O}$  is probed because it prevents vibrational excitation transfer processes from artificially causing decay of the orientational correlation function and observables related to spectral diffusion.<sup>35,36</sup> MD simulations indicate that a dilute amount of HOD does not perturb the structure and properties of  $\text{H}_2\text{O}$  and that the OD stretch reports on the dynamics of water.<sup>37</sup> The laser system used to generate the infrared light that excites the OD hydroxyl stretch consists of a Ti:Sapphire oscillator that seeds a regenerative amplifier. The output of the regenerative amplifier pumps an optical parametric amplifier, which generates near-infrared wavelengths that are difference frequency mixed in a  $\text{AgGaS}_2$  crystal. The resulting mid-infrared pulses are centered at  $\sim 4 \mu\text{m}$  ( $2500 \text{ cm}^{-1}$ ) but are tuned to the peak of the absorption spectrum for a given sample (for instance,  $2565 \text{ cm}^{-1}$  for  $w_0 = 2$ ).

The experimental layout and procedures of the two-dimensional infrared (2D IR) vibrational echo experiment have been described in detail elsewhere.<sup>24,38</sup> In brief, the mid-IR light is beam split into three time-ordered excitation beams and a fourth beam called the local oscillator (LO). The first excitation pulse creates a coherence state between the  $v = 0$  and  $v = 1$  vibrational levels of the OD stretch. During the evolution period  $\tau$  that follows, the phase relationships between the oscillators decay. At time  $\tau$ , the second pulse creates a population state in both the  $v = 0$  or  $v = 1$  vibrational levels. The waiting period  $T_w$  elapses before the third pulse arrives to create a final coherence state, partially restoring the phase relationships. The rephasing of the oscillators causes the vibrational echo to be emitted at a time  $t \leq \tau$  after the third pulse. The OD oscillators undergo spectral diffusion during the  $T_w$  period as the molecules sample different environments due to structural evolution of the system. The vibrational echo signal is spatially and temporally overlapped with the LO for heterodyned detection. The heterodyned signal is frequency dispersed by a monochromator and detected on a 32 element mercury cadmium telluride detector. At a series of fixed  $T_w$  values,  $\tau$  is scanned to generate 2D IR spectra. The time evolution of the spectra as  $T_w$  is increased yields information on spectral diffusion.

Spectral diffusion may be described by the FFCF, which can take the form

$$C_1(t) = \langle \delta\omega_{10}(t)\delta\omega_{10}(0) \rangle = \frac{\delta(t)}{T_2^*} + \sum_i \Delta_i^2 e^{-t/\tau_i} \quad (1)$$

The  $\Delta_i$  are the frequency fluctuation amplitudes of each component, and the  $\tau_i$  are their associated time constants. If the product  $\Delta\tau$  is less than 1 for a given component in the FFCF, then  $\Delta$  and  $\tau$  cannot be determined separately and instead contribute a motionally narrowed homogeneous component to the absorption spectrum with a pure dephasing line width of  $\Gamma^* = \Delta^2\tau = 1/\pi T_2^*$ , where  $T_2^*$  is the pure dephasing time. Contributions from vibrational lifetime, orientational relaxation, and pure dephasing may be combined into the total homogeneous dephasing time,  $T_2$ , which is given by

$$\frac{1}{T_2} = \frac{1}{T_2^*} + \frac{1}{2\tau_{\text{vib}}} + \frac{1}{3\tau_{\text{or}}} \quad (2)$$

where  $T_2^*$ ,  $\tau_{\text{vib}}$ , and  $\tau_{\text{or}}$  are the pure dephasing time, vibrational lifetime, and orientational relaxation time, respectively. The total homogeneous line width is given by  $\Gamma = 1/\pi T_2$ .

The FFCF (eq 1) can be determined from the  $T_w$  dependence of the 2D IR correlation spectra via center line slope (CLS) analysis.<sup>38–40</sup> In this technique, the 2D correlation spectrum at a given  $T_w$  is sliced parallel to the  $\omega_m$  axis (the vertical detection axis) over a range of frequencies about the 2D IR center. Each slice is fit to a Gaussian line shape function to obtain its peak position. This particular variant of the CLS method is known as  $\text{CLS}\omega_m$ . The peak positions are plotted versus the  $\omega_r$  frequencies (the horizontal initial excitation axis) that the slices intercept. The set of peak positions ( $\omega_r, \omega_m$ ) are referred to as center line data. The resulting line is fit with a linear regression to find the slope. Slopes of this nature are obtained for each  $T_w$ . From the plot of slopes versus  $T_w$ , the FFCF can be determined. The procedures describing the extraction of the FFCF from CLS data have been detailed previously.<sup>39</sup> In brief, the CLS decay is fit with a multiexponential decay. The decay constants are the FFCF decay constants. To obtain the homogeneous component of the FFCF, amplitudes and time constants of the CLS are used to simultaneously fit the CLS data and the system's linear FT IR absorption spectrum. The FT IR spectrum is fit via the Fourier transform of the linear response function. A homogeneous component is also included in the fit so that the full FFCF is determined.

The  $\text{CLS}\omega_m$  method is a convenient tool for obtaining the FFCF of a system because it avoids using the nonlinear response function formalism to fit the 2D IR data, and it is insensitive to finite pulse durations, sloping background absorption, Fourier filtering methods (such as apodization), and overlap between the 0–1 and 1–2 transition peaks.<sup>39,40</sup> However, it should be noted that the CLS methodology was developed under the assumption of Gaussian fluctuations.<sup>39,40</sup> In systems such as bulk water, non-Condon effects and deviations from Gaussian fluctuations may influence experimental spectral observables to some extent.<sup>41,42</sup> Non-Condon effects account for a varying transition dipole with absorption frequency.<sup>41,42</sup> MD simulations have shown that the variations in calculated observables obtained via different water models are just as large as simulations that do or do not use the Gaussian approximation.<sup>28,42–44</sup> In aqueous systems that are even more complex than bulk water, such as water nanopools in reverse micelles, it is extremely difficult to extract usable information from 2D spectra using simulations alone. While obtaining the FFCF via the CLS method involves certain approximations, the CLS is still an easily accessible experimental observable that can discern time scales of structural fluctuations and can be used to compare different systems. Furthermore, the CLS is a valid observable that can be the target of simulations regardless of whether it is used to determine the FFCF.

While the focus of this paper is 2D IR vibrational echo experiments, we also report results from polarization and wavelength selective pump–probe experiments, which determine the vibrational lifetime and orientational relaxation time of water molecules inside the reverse micelle environments. In these experiments, the IR light is split into a weak probe pulse and an intense pump pulse. The pump is polarized at  $45^\circ$  relative to the horizontally polarized probe. The two beams cross in the sample, and the parallel and perpendicular components ( $\pm 45^\circ$ ) of the probe are resolved using a computer-controlled rotation

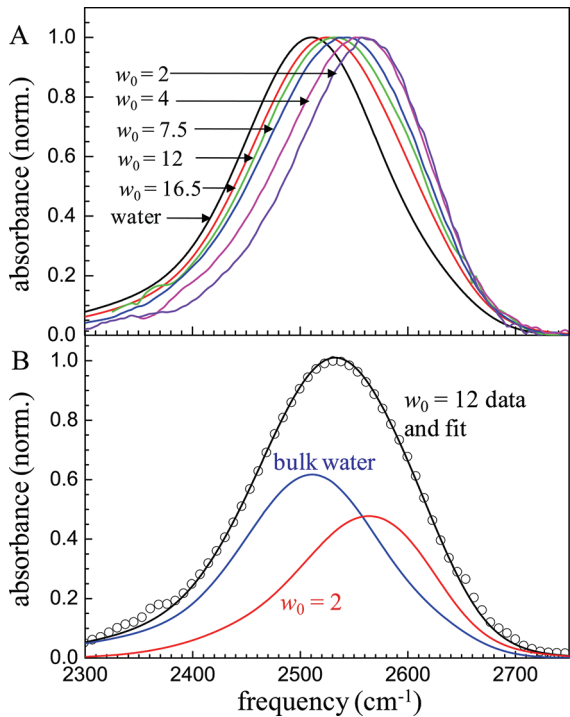


**Figure 2.** (A) Linear FTIR absorption spectra for the range of reverse micelle sizes studied, in addition to bulk water. The smaller reverse micelles,  $w_0 = 2, 4$ , and  $7.5$  were made in carbon tetrachloride, while  $w_0 = 12$  and  $16.5$  were made in cyclohexane. There is a systematic blue shift of the spectra as water content decreases. (B) Two component decomposition of the AOT  $w_0 = 12$  spectrum into the bulk water (blue) and AOT  $w_0 = 2$  (red) spectra. The black dots are the original spectrum, and the black line is the two-component fit.

stage. Before entering the monochromator, the polarization of the probe is set to horizontal to eliminate problems from diffraction and reflection efficiencies of the optics inside the monochromator for different polarizations. The frequency dispersed signal is detected on the 32 element mercury cadmium telluride detector. The measured parallel and perpendicular signals yield information about the population relaxation and orientational dynamics of the water molecules (HOD) and are given by

$$I_{\parallel}(t) = P(t)(1 + 0.8C_2(t)) \quad (3)$$

$$I_{\perp}(t) = P(t)(1 - 0.4C_2(t)) \quad (4)$$

where  $P(t)$  is the vibrational population relaxation and  $C_2(t)$  is the second Legendre polynomial orientational correlation function for a dipole transition. These two signals may be combined to yield the pure population relaxation,

$$P(t) = I_{\parallel}(t) + 2I_{\perp}(t) \quad (5)$$

The anisotropy, from which  $C_2(t)$  may be extracted, is given by

$$r(t) = \frac{I_{\parallel}(t) - I_{\perp}(t)}{I_{\parallel}(t) + 2I_{\perp}(t)} = 0.4C_2(t) \quad (6)$$

For two-component systems consisting of bulk-like water in the core and water at the interface of large reverse micelles, eqs 5 and 6 must be extended, as discussed below, to account for the contributions of different subensembles of water molecules. As

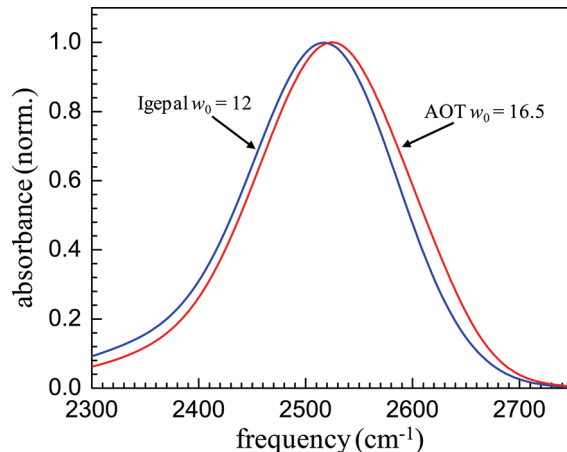


**Figure 3.** Linear FT IR absorption spectra for Igepal  $w_0 = 12$  (blue) AOT  $w_0 = 16.5$  (red). Even though these two reverse micelles both have a 5.8 nm water pool diameter, the Igepal spectrum is red-shifted because the headgroup regions are different between the two surfactants.

with the CLS methodology discussed above, eqs 3–6 are somewhat approximate, as MD studies have suggested that non-Condon effects, excited-state absorption, and spectral diffusion influence the anisotropy to some extent.<sup>45,46</sup> However, differences in simulation models and electrostatic maps can produce errors comparable to differences between simulations that do or do not use the Gaussian approximation or implement non-Condon effects.<sup>28,42–45</sup> As a result, the data analysis implemented here provides viable information concerning the dynamics of water molecules.

### III. RESULTS AND DISCUSSION

**A. Linear Absorption and Pump–Probe Spectroscopy.** Figure 2A displays the FTIR absorption spectra for the OD stretch of HOD in H<sub>2</sub>O in the range of  $w_0$ 's of AOT reverse micelles studied in this work along with bulk water for comparison. The hydrogen bonding interaction between water (HOD) and the sulfonate head groups at the micelle interface causes the OD spectrum to blue shift. As the reverse micelles become smaller, a greater proportion of water molecules interact with the sulfonate head groups and cause a greater blue shift. Previous analysis has shown that the water spectra in AOT reverse micelles can be decomposed into a bulk water spectrum and an interfacial water spectrum. The interfacial spectrum is approximated as the  $w_0 = 2$  spectrum<sup>6,8,10</sup> because in this system virtually all of the water molecules interact with the head groups. In describing the absorption spectrum, the only adjustable parameter is a fractional population corresponding to the amounts of interfacial and bulk water in a given reverse micelle. This model is often referred to as the core/shell or two component model. This model takes the following mathematical form:

$$I_{\text{tot}}(\omega) = a_1 I_1(\omega) + (1 - a_1) I_2(\omega) = S_1(\omega) + S_2(\omega) \quad (7)$$

where  $a_1$  is the fractional population, and  $I_1$  and  $I_2$  are the component spectra for bulk water and  $w_0 = 2$ , respectively. Figure 2B shows the decomposition of the AOT  $w_0 = 12$  spectrum. The blue and red curves are the bulk water and  $w_0 = 2$  spectra, respectively. The circles are the  $w_0 = 12$  spectrum, and

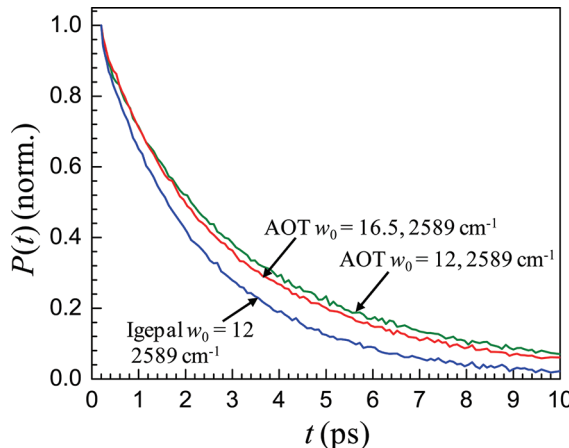


**Figure 4.** Population relaxation decays for AOT  $w_0 = 12$  (green), AOT  $w_0 = 16.5$  (red), and Igepal  $w_0 = 12$  (blue) at a detection wavelength of  $2589 \text{ cm}^{-1}$ . AOT  $w_0 = 12$  has the slowest decay, and Igepal  $w_0 = 12$  has the fastest.

the black curve is the weighted sum of the bulk water and  $w_0 = 2$  spectra. The figure shows excellent agreement for the model embodied in eq 7. For AOT reverse micelles,  $a_1 = 0.56$  for  $w_0 = 12$  and 0.74 for  $w_0 = 16.5$ .

Figure 3 compares the linear FTIR absorption spectra of AOT  $w_0 = 16.5$  and Igepal  $w_0 = 12$ . Both samples have water pool diameters of 5.8 nm. Even though the water pool sizes are identical, the spectra are not the same because the headgroup regions are different. The spectrum for Igepal  $w_0 = 12$  is less blue-shifted than AOT  $w_0 = 16.5$ . The difference is caused by the different nature of the interfacial interactions for the two surfactants.

Population relaxation and rotational dynamics can provide considerable insight into the dynamics and interactions of water molecules in confinement. Population relaxation is described via the vibrational lifetime, a time constant that measures how quickly vibrational energy dissipates in a system. The vibrational energy goes into a combination of low frequency modes, such as bending modes, torsions, and bath modes, that sums to the original energy.<sup>47,48</sup> In bulk water, vibrational energy dissipates relatively easily through these pathways. Confinement or the presence of solutes can modify vibrational relaxation because certain pathways that were available in bulk water may no longer be accessible. As a result, the vibrational lifetime is extremely sensitive to local environments. Figure 4 shows the population decays for AOT  $w_0 = 12$ , AOT  $w_0 = 16.5$ , and Igepal  $w_0 = 12$  at a high detection frequency of  $2589 \text{ cm}^{-1}$ , where the contribution from water at the interface is enhanced. As demonstrated by Moilanen et al., the population decay of water in large reverse micelles can be decomposed into contributions from the bulk water core and the interfacial water molecules at the head groups:

$$P(t) = A_1 e^{-t/\tau_{\text{vib}1}} + (1 - A_1) e^{-t/\tau_{\text{vib}2}} \quad (8)$$

where  $A_1$  is a fractional population and  $\tau_{\text{vib}1}$  and  $\tau_{\text{vib}2}$  are the vibrational lifetimes of bulk water and water at the headgroup interface, respectively. In larger AOT reverse micelles, the time constants do not change with wavelength, but the fractional population  $A_1$  does change with wavelength. In eq 8,  $A_1$  is not the same as  $a_1$  in eq 7 because  $A_1$  changes with wavelength while  $a_1$  is a single value. At all wavelengths,  $\tau_{\text{vib}1}$  is fixed at the literature

**Table 1. Population and Orientational Relaxation Parameters for Large and Intermediate Reverse Micelles<sup>a</sup>**

	AOT $w_0 = 16.5$	AOT $w_0 = 12$	AOT $w_0 = 7.5^b$
$\tau_{\text{vib}1}$ (ps)	1.8	1.8	2.1
$\tau_{\text{vib}2}$ (ps)	4.5	4.7	5.5
$\tau_{\text{or}1}$ (ps)	2.6	2.6	4.4
$\tau_{\text{or}2}$ (ps)	15	23	30

<sup>a</sup> Error bars are  $\pm 0.2$  for  $\tau_{\text{vib}1}$ ,  $\tau_{\text{vib}2}$ , and  $\tau_{\text{or}1}$ ;  $\pm 5$  for  $\tau_{\text{or}2}$ . <sup>b</sup> Data reproduced from ref 24.

**Table 2. Population Relaxation Parameters for Small Reverse Micelles<sup>a,b</sup>**

sample	parameter	$2590 \text{ cm}^{-1}$	$2610 \text{ cm}^{-1}$	$2620 \text{ cm}^{-1}$	$2640 \text{ cm}^{-1}$
AOT $w_0 = 2$	$A_1$	0.13	0.08	0	0
	$\tau_{\text{vib}1}$ (ps)	2.0	2.0		
	$\tau_{\text{vib}2}$ (ps)	7.3	7.5	7.4	8.1
AOT $w_0 = 4$	$A_1$	0.22	0.15	0.13	0.10
	$\tau_{\text{vib}1}$ (ps)	2.0	2.0	2.0	2.0
	$\tau_{\text{vib}2}$ (ps)	6.4	6.6	6.9	7.4

<sup>a</sup> Error bars are  $\pm 0.2$  ps for time constants,  $\pm 0.04$  for amplitudes;  $A_2 = 1 - A_1$ . <sup>b</sup> Data reproduced from ref 24.

value of 1.8 ps for bulk water,<sup>6,8</sup> and  $\tau_{\text{vib}2}$  is determined to be  $\sim 4.5$  ps for both AOT reverse micelle sizes ( $w_0 = 12$  and 16.5), as summarized by Table 1. This interfacial vibrational lifetime is consistent with a previous value obtained for large reverse micelles in isoctane.<sup>6,8</sup> Figure 4 shows that the population decay for AOT  $w_0 = 12$  is slightly slower than that for AOT  $w_0 = 16.5$  at the same wavelength. This behavior arises because there is more interfacial water in AOT  $w_0 = 12$  and therefore a greater contribution of the component with a slower decay. The population decays in Figure 4 have been corrected for a well-understood long time nonzero baseline that arises from the deposition of heat into the system from the vibrational relaxation.<sup>10,13,49–54</sup>

The population relaxation parameters for AOT  $w_0 = 7.5$  are also listed in Table 1, which have been published previously.<sup>24</sup> AOT  $w_0 = 7.5$  can also be decomposed into core and interfacial environments, but the vibrational lifetime associated with the core is slightly slower (2.1 ps) than the value for bulk water (1.8 ps), and the vibrational lifetime at the interface also slows down (5.5 ps). The AOT  $w_0 = 7.5$  reverse micelle is too small to support a purely bulk-like water core, but it is still large enough to have separate environments with different dynamics. The  $w_0 = 7.5$  system can be considered an intermediate-sized reverse micelle. In the spectral diffusion analysis in the next section, AOT  $w_0 = 7.5$  will be analyzed in two ways as both a small and large reverse micelle.

Table 2 lists the vibrational relaxation parameters for smaller reverse micelles, AOT  $w_0 = 2$  and  $w_0 = 4$ . These reverse micelles present a situation where, even though the water molecules exist in a mainly interfacial environment without a core region, the vibrational lifetime still has two components. For both reverse micelles, there is one lifetime of 2 ps and a slower lifetime of  $\sim 7$  ps for  $w_0 = 2$  and  $\sim 6.5$  ps for  $w_0 = 4$ . The faster (2 ps) lifetime is attributed to OD hydroxyls that are hydrogen bonded to the oxygens of water molecules, while the second, slower lifetime is attributed to ODs bound to head groups.

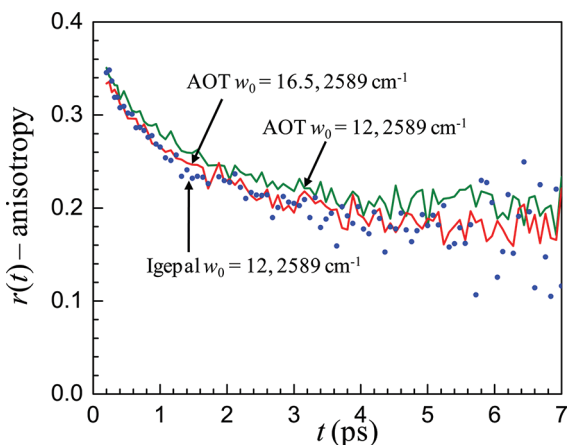


**Figure 5.** Anisotropy (orientational relaxation) data for AOT  $w_0 = 12$  (green line), AOT  $w_0 = 16.5$  (red line), and Igepal  $w_0 = 12$  (blue dots) at a detection wavelength of  $2589\text{ cm}^{-1}$ . All sets of data display a plateau that is characteristic for multicomponent anisotropy decays.

Unlike the larger reverse micelles, there is a frequency dependence to the value of the second, longer lifetime. As the frequency increases, the population of the 2 ps lifetime decreases, and the value of the slower lifetime increases. At the highest frequencies for AOT  $w_0 = 2$ , the population decay becomes single exponential because only ODs bound to head groups are observed. The two component behavior arises because the vibrational lifetime is extremely sensitive to local environments. The water molecules in the small reverse micelles are mostly hydrogen bonded to the interface, but they can sometimes form hydrogen bonds to other water molecules. These water–hydroxyl interactions give rise to the faster lifetime, while water–interface interactions give rise to the slower lifetime. As the frequency is tuned to the blue, the nature of the OD-headgroup interactions changes, which is reflected in an increasingly long lifetime.

Orientational relaxation, determined from the time-dependent anisotropy (eq 6), provides information on how quickly water molecules rotate. In the mechanism for hydrogen bond reorientation, large amplitude rotations occur via concerted motions of the water molecules.<sup>1,2</sup> Interfaces and solute molecules can modify water orientational relaxation.<sup>5–8,10–14,26</sup> Like the population dynamics, Moilanen et al. found that the anisotropy decay of water inside of large reverse micelles can be decomposed into two components.<sup>6,8</sup> The two-component anisotropy model takes on a more complicated form than the two-component population decay:<sup>5,8,10</sup>

$$r(t) = \frac{A_1 e^{-t/\tau_{vib1}} e^{-t/\tau_{or1}} + (1 - A_1) e^{-t/\tau_{vib2}} e^{-t/\tau_{or2}}}{A_1 e^{-t/\tau_{vib1}} + (1 - A_1) e^{-t/\tau_{vib2}}} \quad (9)$$

where  $A_1$ ,  $\tau_{vib1}$ , and  $\tau_{vib2}$  are defined by eq 8, and  $\tau_{or1}$  and  $\tau_{or2}$  are the orientational relaxation time constants for bulk water and interfacial water, respectively. Because  $A_1$ ,  $\tau_{vib1}$ , and  $\tau_{vib2}$  can be determined separately via the population decay and  $\tau_{or1} = 2.6$  ps from the literature,<sup>54</sup>  $\tau_{or2}$  is the only adjustable parameter in eq 9. Typically, anisotropy decays for several wavelengths are fit simultaneously to extract  $\tau_{or2}$ .<sup>5,6,8,9</sup> For large reverse micelles,  $\tau_{or2}$  is  $\sim 20$  ps, which is much slower than the bulk water orientational relaxation time of 2.6 ps. The two-component anisotropy decays display an apparent plateau

beginning at  $\sim 4$  ps,<sup>5,8</sup> as seen in Figure 5. The plateau is a result of the different lifetimes and orientational relaxation times for bulk and interfacial water. At sufficiently long time, the anisotropy will decay to zero, but this time is outside the experimental time window, which is limited by the vibrational lifetimes.

AOT  $w_0 = 7.5$  also follows the two-component anisotropy decay model, but similar to the population relaxation behavior, the time constants for the core region are slightly slower.<sup>24</sup> The orientational relaxation time for the interface is also slower than its counterpart in the larger reverse micelles. In addition to summarizing the population relaxation parameters for AOT  $w_0 = 16.5$ , 12, and 7.5, Table 1 also lists the orientational relaxation parameters for these three systems. The orientational relaxation decays for the small reverse micelles ( $w_0 = 2$  and 4) follow a wobbling-in-a-cone model,<sup>10,19,55</sup> which consists of a short  $\sim 1$  ps time constant decay followed by a very slow component decay of  $\sim 100$  ps.<sup>6,24</sup> These time scales reflect different types of angular motions of the water molecules and not dynamics in different subensembles. Even though the population decays for the small reverse micelles follow a two component model, the anisotropy decays do not. The essentially single ensemble orientational relaxation behavior for the smallest reverse micelles is evidenced by a lack of wavelength dependence for the decays.<sup>6,24</sup> The lifetime for the smallest reverse micelles depends on the hydrogen bonding of the OD hydroxyl, which is either to a sulfonate or to a water oxygen. However, the orientational relaxation depends on the concerted motion of many water molecules. Because all of the water molecules in the smallest reverse micelles are either bound to the interface or are bound to a water that is bound to the interface, none are truly independent of the influences of the interface. For orientational relaxation, the water nanopools of the smallest reverse micelles behave essentially as a single ensemble.

Figures 4 and 5 also display data for the Igepal  $w_0 = 12$  reverse micelles, which have the same water pool diameter as AOT  $w_0 = 16.5$ . An Igepal reverse micelle is different from an AOT reverse micelle because the hydroxyl head groups can exchange with HOD molecules in the water pool. The exchange of deuterium with the headgroup interface creates a third vibrational species, deuterated hydroxyl head groups, that contributes to the population decay and anisotropy signals. The overall population of OD head groups is generally very small, but these head groups make a small contribution to the signal. The three component treatment of Igepal reverse micelles has been discussed in detail previously.<sup>17</sup> The population decay for Igepal in Figure 4 indicates that even though the reverse micelles are of the same size, the population dynamics in Igepal are slightly faster than those in AOT. The curve for Igepal  $w_0 = 12$  decays more quickly than in AOT  $w_0 = 16.5$ . Table 3 lists the population and orientation relaxation parameters for Igepal  $w_0 = 12$ . The parameters with a subscript of 1 are the bulk water core parameters, parameters with a subscript of 2 are for waters at the interface, and parameters with a subscript of 3 are for OD head groups. While the bulk water component is the same regardless of the surfactant identity, the vibrational lifetime for waters at the Igepal interface is faster than the interfacial vibrational lifetime in AOT. The vibrational lifetime of the OD head groups is similar to that for waters at the AOT interface and is similar to previous measurements.<sup>17</sup> There is no orientational time constant given for the OD head groups

Table 3. Population and Orientational Relaxation Parameters for Igepal  $w_0 = 12^a$ 

$A_1$	$\tau_{\text{vib}1}$ (ps)	$\tau_{\text{or}1}$ (ps)	$A_2$	$\tau_{\text{vib}2}$ (ps)	$\tau_{\text{or}2}$ (ps)	$A_3$	$\tau_{\text{vib}3}$ (ps)
$0.71 \pm 0.02$	$1.8 \pm 0.2$	$2.6 \pm 0.2$	$0.25 \pm 0.02$	$3.7 \pm 0.3$	$15 \pm 3$	$0.04 \pm 0.02$	$4.1 \pm 0.3$

<sup>a</sup> Subscript 1 – bulk water; subscript 2 – interfacial water; subscript 3 – OD head groups.

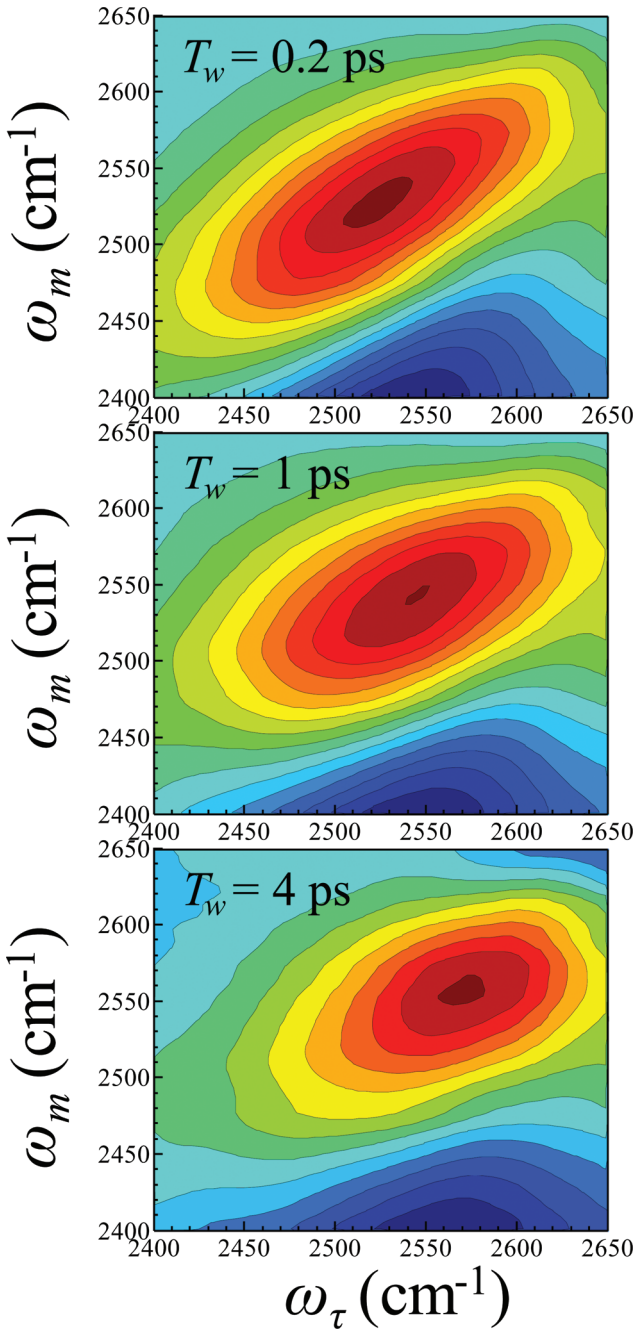


Figure 6. 2D IR correlation plots for AOT  $w_0 = 16.5$  at  $T_w = 0.2, 1$ , and  $4$  ps. At early  $T_w$  the spectra are quite elongated, but the spectra do not complete spectral diffusion by the end of the experimental  $T_w$  window.

because it will be exceedingly slow; it is assumed that it is equivalent to the overall rotation time of the reverse micelle, which occurs on the order of nanoseconds. The anisotropy decays in Figure 5 indicate that there is little difference between

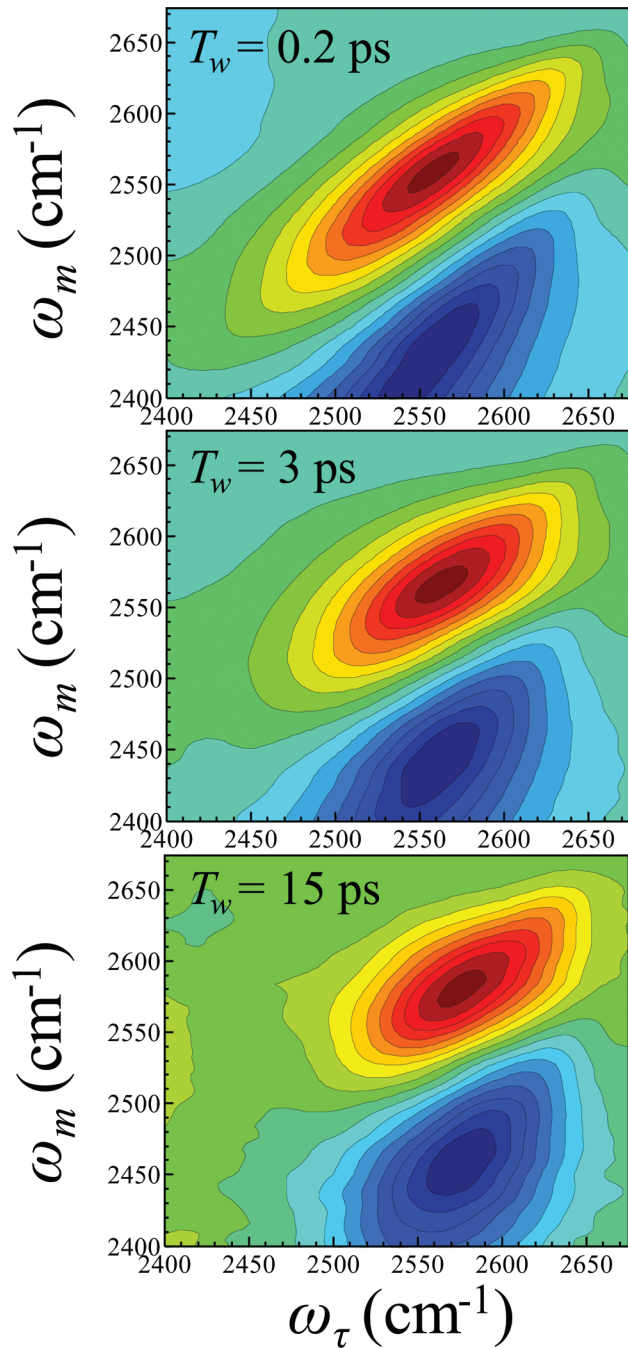


Figure 7. 2D IR correlation plots for AOT  $w_0 = 2$  at  $T_w = 0.2, 3$ , and  $15$  ps. At early  $T_w$  the spectra are quite elongated, but the spectra do not complete spectral diffusion by the end of the experimental  $T_w$  window. Data may be taken out longer for AOT  $w_0 = 2$  because of the sample's longer vibrational lifetime. The data has been reproduced from ref 24.

the rotational behaviors in Igepal and in AOT reverse micelles of the same size, as the curves are virtually identical. However,

**Table 4. Exponential Fit Parameters to Raw CLS Data for Large and Intermediate Reverse Micelles<sup>a</sup>**

$w_0$	$a_0$	$a_1$	$t_1$ (ps)	$a_2$	$t_2$ (ps)	$y_0$
7.5	0.30	0.14	1.1	0.47	6.4	0.09
12	0.28	0.57	2.5			0.15
16.5	0.37	0.34	2.1			0.29

<sup>a</sup>  $a_0$ —drop from 1;  $a_i$ —amplitude;  $t_i$ —time constant;  $y_0$ —offset. Error bars are  $\pm 0.02$  for  $a_0$ ,  $a_i$  and  $y_0$ ;  $\pm 0.2$  for  $t_1$ ,  $\pm 1$  for  $t_2$ .

because the small effects from the OD head groups in Igepal must be taken into account, it cannot be concluded that the actual dynamics in AOT and Igepal are exactly the same. Nonetheless, it is clear that interaction with the interface significantly affects the rotational dynamics of water, while the chemical composition of the interface has substantially less influence.

**B. Spectral Diffusion in Large Reverse Micelles.** 2D IR vibrational echo correlation spectra were measured for each of the reverse micelles (AOT  $w_0 = 16.5, 12, 7.5, 4$ , and 2 and Igepal  $w_0 = 12$ ). 2D correlation spectra for AOT  $w_0 = 16.5$  at a series of  $T_w$ 's are shown in Figure 6 and for AOT  $w_0 = 2$  in Figure 7. These samples provide representative spectra for the large and small reverse micelles, respectively. Each spectrum consists of two peaks. The positive (red) peak along the diagonal corresponds to the 0–1 vibrational transition, while the negative (blue) peak off the diagonal arises from vibrational echo emission at the 1–2 transition frequency. The 1–2 peak appears off the diagonal and shifted along the  $\omega_m$  axis due to the vibrational anharmonicity. At early  $T_w$  values, the spectra are elongated along the diagonal, showing a strong correlation that an oscillator excited at a certain frequency will retain that frequency after a short amount of time. The spectra become more symmetric as  $T_w$  lengthens, and the water molecules undergo spectral diffusion because of structural evolution of the system. Bulk water generally completes spectral diffusion within a few picoseconds.<sup>43,44</sup> By 2 ps, the shape of the bulk water spectrum has evolved from diagonally elongated to nearly symmetric (circular). By contrast, none of the reverse micelles, from  $w_0 = 2$  through  $w_0 = 16.5$ , exhibit symmetric spectra at the end of their experimental  $T_w$  ranges, indicating that spectral diffusion is not completed.

The large reverse micelles ( $w_0 = 12$  and 16.5) and intermediate reverse micelles ( $w_0 = 7.5$ ) contain two types of water molecules: core waters and interfacial waters. As shown by FTIR analysis, each of these regions is characterized by its own absorption spectrum (see Figure 2B). In a 2D IR experiment, each of these ensembles generates a 2D IR spectrum. The overall measured 2D spectrum is a combination of the individual spectra. When the peak separation between components is relatively small, the individual spectra are not resolved, and the 2D IR correlation plots look as if there is a single species. In large reverse micelles, the component spectra are bulk water and  $w_0 = 2$  (see Figure 2B).

We have shown recently that the CLS method can be extended to two-component systems.<sup>56</sup> Each two-component 2D spectrum can be decomposed into its constituent spectra, and each of these spectra has a characteristic CLS decay. In large reverse micelles, the bulk water CLS is known, so it is possible to obtain the CLS decay (and by extension, the FFCF) of the interfacial waters. In a system with two ensembles of vibrations, i.e., bulk and interfacial water OD hydroxyl stretches, simply applying the CLS method (calculating the slope around the

2D IR maximum location) does not provide information on the interfacial water dynamics.<sup>56</sup> The resulting multiexponential fit to the CLS curve yields a combination of the time constants of the bulk water and interfacial water CLS decays that cannot be directly resolved into the time constants and amplitudes for each ensemble.

The recent theoretical work developed in a previous publication<sup>56</sup> demonstrated that it is possible to extract the unknown CLS and FFCF of one component if the CLS for the other component is known; in this case, the FFCF and CLS for bulk water are known. It was found that for the two-component 2D IR spectrum (also called the combined spectrum), the peak positions ( $\omega_{mC}^*$ ) of slices parallel to the  $\omega_m$  axis are weighted combinations of the peak positions ( $\omega_{m1}^*$ ) of the bulk water spectrum and the peak positions ( $\omega_{m2}^*$ ) of a second component:

$$\begin{aligned}\omega_{mC}^*(\omega_m, \omega_\tau, T_w) = & f_1(\omega_\tau, T_w)\omega_{m1}^*(\omega_m, \omega_\tau, T_w) \\ & + (1 - f_1(\omega_\tau, T_w))\omega_{m2}^*(\omega_m, \omega_\tau, T_w)\end{aligned}\quad (10)$$

In the case of large reverse micelles, this second component is the ensemble of interfacial water molecules. The set of peak positions for the slices are also known as center line data. In eq 10,  $f_1$  is the fractional population of bulk water, which is both  $T_w$ - and frequency-dependent. This fraction term may be obtained from the FTIR absorption spectra of the two components and the measured vibrational lifetimes:

$$f_1(\omega_\tau, T_w) = \frac{S_1(\omega_\tau)e^{-T_w/\tau_{vib1}}}{S_1(\omega_\tau)e^{-T_w/\tau_{vib1}} + S_2(\omega_\tau)e^{-T_w/\tau_{vib2}}}\quad (11)$$

where  $S_1$  and  $S_2$  are defined by eq 7. Since center line data for the combined system and bulk water can be measured separately, eq 10 can be rearranged to obtain  $\omega_{m2}^*$  for the interface:

$$\omega_{m2}^*(\omega_m, \omega_\tau, T_w) = \frac{(\omega_{m2C}^*(\omega_m, \omega_\tau, T_w) - f_1(\omega_\tau, T_w)\omega_{m1}^*(\omega_m, \omega_\tau, T_w))}{(1 - f_1(\omega_\tau, T_w))}\quad (12)$$

For eq 12 to work, the  $f_1$  fraction term must be known, which requires that the vibrational lifetimes are known. In addition, the peak position of the interfacial water must also be known, or reasonably approximated. When CLS analysis is applied to the calculated interfacial water center line data, the CLS will be calculated around the peak position of the interface water band, not the 2D IR maximum. As shown in Figure 2B, the  $w_0 = 2$  spectrum is an excellent approximation for the interfacial water spectrum. For  $w_0 = 2$ , the peak position is  $2565\text{ cm}^{-1}$ .

The raw CLS data that has not been decomposed into separate contributions (calculated around the 2D IR centers for each correlation plot) for the AOT  $w_0 = 16.5$  and 12 systems each fit well to a single exponential to an offset. The raw CLS data for AOT  $w_0 = 7.5$  fit well to a biexponential decay with an offset. The fit parameters to these curves are given in Table 4. In addition to amplitudes and time constants, and differences between 1 and the initial values at  $T_w = 0$  are given as the  $a_0$  term in the table. From these fit parameters, the raw CLS data may be reconstructed. These parameters do not reflect the dynamics of either component of the two-component system. However, they will be useful to compare an MD simulation of the entire system to the measured experimental data.

Figure 8 shows the results of eq 12 when applied to AOT  $w_0 = 12$  at  $T_w = 0.2\text{ ps}$ . The black circles are the actual measured

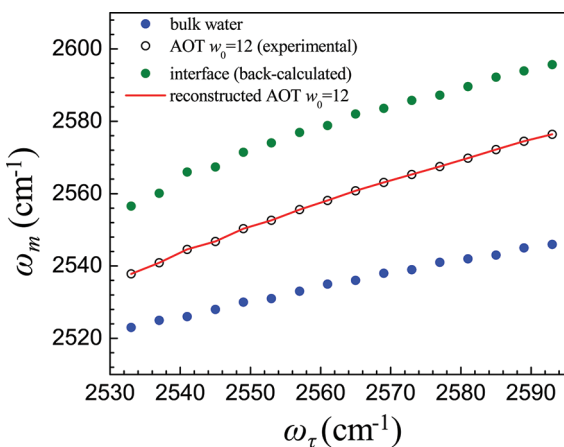


**Figure 8.** Representative center line data for the back-calculation of the interfacial CLS. Shown here are results for AOT  $w_0 = 12$  at  $T_w = 0.2$  ps. The blue dots are bulk water center line data, and the black circles are the experimentally measured center line data for AOT  $w_0 = 12$  at  $T_w = 0.2$  ps. The green dots are the back-calculated interfacial center line data using eq 12. The red line is the recombination of the back-calculated interfacial data with the bulk water data to reproduce the experimental data.

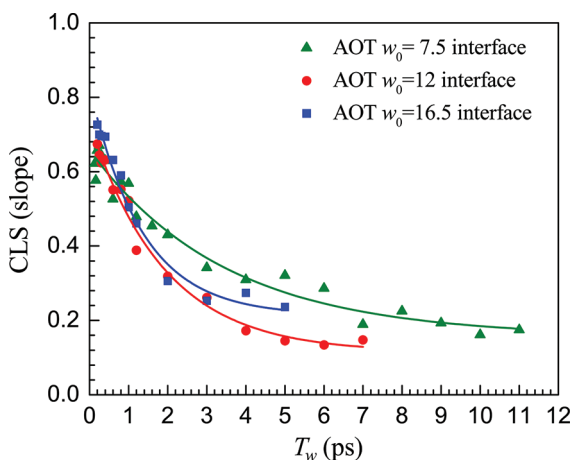


**Figure 9.** Interfacial CLS data for AOT  $w_0 = 16.5, 12$ , and  $7.5$ . The lines through the data are the calculated interfacial FFCFs.

experimental center line data for the AOT  $w_0 = 12$  reverse micelle. The blue dots are the center line data for bulk water, which was obtained separately. The bulk water CLS was used to determine the bulk water FFCF, which was then used to obtain the bulk water CLS for longer times because experimental data can only be measured out to 2 ps due to the lifetime limitations.<sup>56</sup> The green dots are the interfacial water center line data found by applying eq 12. The red line is a verification of the algorithm. The calculated interfacial water center line data and the center line data for bulk water are recombined with the fraction terms to make sure that the original combined center line data is reproduced. Because eq 12 is simple linear algebra, the agreement is virtually quantitative.

Center line data for the interface, as displayed by Figure 8, were obtained for AOT  $w_0 = 16.5, 12$ , and  $7.5$  at all measured  $T_w$ 's. The interfacial CLS curves for these three micelles are displayed in Figure 9. Overall, the interfacial CLS curves are very similar for  $w_0 = 12$  and  $16.5$ . The lack of a size dependence for the

**Table 5. Interfacial FFCF Parameters for Large and Intermediate Reverse Micelles<sup>a</sup>**

$w_0$	$\Gamma$ (cm <sup>-1</sup> )	$\Delta_1$ (cm <sup>-1</sup> )	$\tau_1$ (ps)	$\Delta_S$ (cm <sup>-1</sup> )
7.5	57	44	3.5	24
12	35	55	1.9	21
16.5	28	50	1.3	29

<sup>a</sup> Error bars are  $\pm 5$  for  $\Gamma$  and  $\Delta$ 's;  $\pm 0.5$  for  $\tau_1$ .

large reverse micelles is consistent with a lack of size dependence for the interfacial orientational relaxation and the vibrational lifetime.<sup>6,8</sup> The  $w_0 = 7.5$  system is considerably smaller in size, and its interfacial CLS seems to decay slightly slower than the larger reverse micelles. It should be noted that the bulk water center line data were used in the  $w_0 = 7.5$  calculation, even though our experiments suggest that the core is not exactly like bulk water. We cannot measure the core of the  $w_0 = 7.5$  reverse micelle directly, so bulk water is the best approximation for use in the calculation.

The interfacial CLS curves fit well to a single exponential decay plus an offset. The FFCFs for  $w_0 = 16.5, 12$ , and  $7.5$  were calculated by simultaneously fitting the CLS curve and the  $w_0 = 2$  spectrum for each sample. Table 5 summarizes the FFCF parameters for the large reverse micelles and  $w_0 = 7.5$ . As suggested by examination of the CLS curves,  $w_0 = 12$  and  $16.5$  yield very similar FFCF parameters. This similarity indicates that, like the rotational and population relaxation dynamics,<sup>6,8</sup> spectral diffusion at the interface in large reverse micelles is independent of size. For large reverse micelles, there is a core of bulk-like water, and the curvature of the interface is mild. The solvation of the head groups is independent of size.<sup>6,8,9</sup> The result is that the local water–interface interactions and dynamics do not change with size for sufficiently large reverse micelles.

The exponential decay portion of the FFCF for  $w_0 = 12$  and  $16.5$  is  $\sim 1.6$  ps, which is within experimental error, very similar to the FFCF long time constant of bulk water, 1.7 ps. The 1.7 ps time constant in bulk water is attributed to global hydrogen bond rearrangement.<sup>43,44</sup> In the analysis of the orientational relaxation, lifetimes, and spectra of interfacial water in large AOT reverse micelles, it was shown that the interfacial layer is approximately one water molecule thick.<sup>6,8</sup> This conclusion was supported by the observation that the populations of bulk water and interfacial water obtained from both the analysis of the absorption spectra and from amplitude fractions found from the biexponential population decays matched the fractions of each region obtained by geometrically approximating the interfacial layer as a shell 2.8 Å thick, which is roughly the effective diameter of one water molecule.<sup>8</sup> That only the first solvation shell is strongly perturbed by the interfaces is supported by other experiments.<sup>3,57</sup> Some studies have suggested that the hydration layer around proteins can extend out to  $\sim 10$  Å.<sup>58</sup> However, it should be noted that experimental evidence for this observation is lacking and that such large hydration layers are generally found via MD simulations.<sup>58–60</sup>

It was found that for large reverse micelles, the orientational relaxation time is slow at the interface,  $\sim 20$  ps.<sup>6,8,9</sup> This suggests that the exchange of water between the interfacial region and the bulk-like core occurs on this time scale or slower since exchange will not occur without changes in orientation. Therefore, on a time scale of 1.6 ps, there is a fixed ensemble of interfacial water molecules that are bound to the sulfonate head groups but will

also be interacting with water molecules that are beyond the interfacial layer.

Water molecules at the interface are hydrogen bonded to water molecules beyond the interfacial layer, and the frequency of the interfacial water molecules will be influenced by the dynamics of this more bulk-like water. Noninterfacial water molecules will be making and breaking hydrogen bonds with the interfacial water molecules as well as with other core water molecules. It is possible that the  $\sim 1.6$  ps component of the interfacial water FFCF is produced by the hydrogen bond rearrangement of noninterfacial water molecules that are making and breaking hydrogen bonds with the interfacial water molecules. This proposition, if correct, indicates that water molecules immediately beyond the interfacial layer behave very much like bulk water. Although these water molecules would have hydrogen bonds to interfacial water molecules, they also interact with a large collection of basically bulk-like core water molecules. Again, it is important to point out that assigning the fast component of the interfacial FFCF to the hydrogen bond dynamics of noninterfacial water molecules is a conjecture based on the similarity of the observed interfacial spectral diffusion dynamical time scale and the known time scale for bulk water hydrogen bond randomization.

In contrast to bulk water, the interfacial FFCF has an offset. The offset is produced by dynamics that are too slow to measure because they are outside the experimental time window that is set by the vibrational lifetime. It is not surprising that the interfacial water has very slow dynamics. Complete spectral diffusion within the interfacial inhomogeneous line requires sampling all of the frequencies (see Figure 2B). As shown in Table 2, the vibrational lifetime of the  $w_0 = 2$  reverse micelle becomes longer at the very blue side of the absorption line. This shows that the interface is not a single environment. All environments must be sampled for spectral diffusion to be complete. As mentioned above, the interfacial orientational relaxation time for large reverse micelles is  $\sim 20$  ps. Orientational relaxation will require breaking a hydrogen bond to the interface (sulfonate headgroup). Therefore, it is reasonable to conclude that the time required for a water molecule to sample the range of interfacial environments will be quite slow.

For spectral diffusion to be truly complete, all frequencies must be sampled, including both the interfacial frequencies and the core frequencies. Thus, there must be exchange between the interfacial and core populations. Molecules at the interface will have to move away from the interface and become core molecules, and core water molecules will have to move toward the head groups and become interfacial water molecules. Again, given the  $\sim 20$  ps interfacial orientational relaxation time, the time scale for interfacial-core exchange should be slow.

The exponential decay of the  $w_0 = 7.5$  FFCF has a time constant of  $\sim 3.5$  ps, which is significantly slower than that observed for the large reverse micelles.  $w_0 = 7.5$  is an intermediate size. The water nanopool in  $w_0 = 7.5$  has a core that is well separated from the interface, but the core has water properties that are somewhat different from bulk-like water. Coupling of the slow dynamics at the interface to water throughout the small nanopool slows the orientational relaxation at both the interface and in the core as well as slowing vibration relaxation in both regions (see Table 1). The 3.5 ps component of the  $w_0 = 7.5$  FFCF may reflect hydrogen bond rearrangement of core water molecules that are bonded to interfacial water molecules. The slowing of this component of

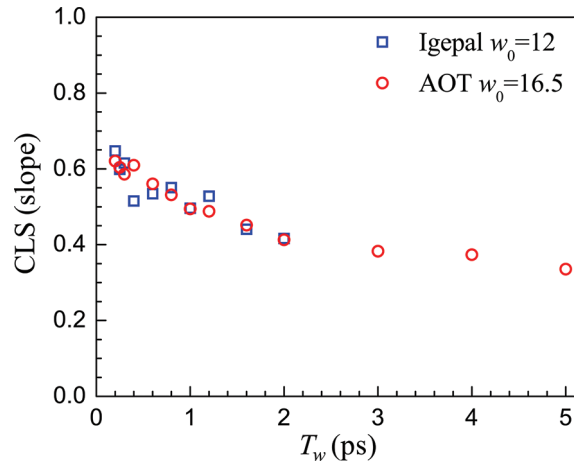


**Figure 10.** CLS data for Igepal  $w_0 = 12$  (blue squares) and AOT  $w_0 = 16.5$  (red circles), showing close agreement between the samples. The CLS data presented in this figure have not been analyzed with the modified two-component CLS model.

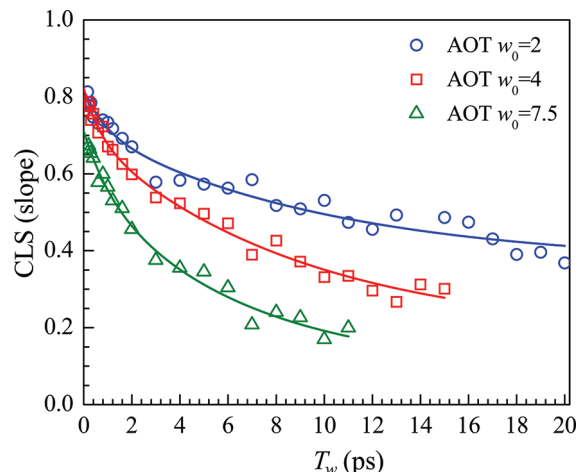


**Figure 11.** CLS data for small reverse micelles, AOT  $w_0 = 2, 4$ , and 7.5. The lines through the data are the calculated FFCFs. As reverse micelle size decreases, spectral diffusion slows down.

the FFCF would be in accord with the slowing of the core water structural dynamics as evidenced by the slower orientational relaxation time.

**C. Spectral Diffusion in Igepal Reverse Micelles.** 2D IR spectra were also measured for Igepal  $w_0 = 12$ , a reverse micelle with the same water pool diameter as AOT  $w_0 = 16.5$ . Because of lifetime limitations, data for AOT  $w_0 = 16.5$  can be taken out to about 5 ps, but the echo signal for Igepal  $w_0 = 12$  is not reliable past 2 ps. Given the limited experimental time window for Igepal, it was impractical to apply eq 12 and obtain an interfacial CLS. Instead, the AOT  $w_0 = 16.5$  and Igepal  $w_0 = 12$  were analyzed with the CLS method in the traditional manner, that is, as if there were a single ensemble. The CLS was obtained around the 2D IR maxima for each  $T_w$ . Figure 10 displays these CLS curves. For the limited range of  $T_w$ 's that could be measured, the CLS for the two samples are almost identical. Given the small experimental time window, our limited results suggest that, at least at early times, spectral diffusion is not too sensitive to the chemical nature of the interface. This result is consistent with the similarity found for

**Table 6.** FFCF Parameters for Small and Intermediate Reverse Micelles

$w_0$	$\Gamma$ ( $\text{cm}^{-1}$ )	$\Delta_1$ ( $\text{cm}^{-1}$ )	$\tau_1$ (ps)	$\Delta_2$ ( $\text{cm}^{-1}$ )	$\tau_2$ (ps)	$\Delta_s$ ( $\text{cm}^{-1}$ )
2	$33 \pm 5$	$19 \pm 2$	$0.9 \pm 0.1$	$36 \pm 1$	$10 \pm 1$	$37 \pm 1$
4	$33 \pm 5$	$21 \pm 2$	$0.7 \pm 0.4$	$44 \pm 5$	$8.9 \pm 3$	$26 \pm 1$
7.5	$57 \pm 2$	$25 \pm 2$	$1.1 \pm 0.2$	$47 \pm 3$	$6.4 \pm 1$	$20 \pm 2$

the interfacial orientational relaxation times of water in AOT and Igepal reverse micelles.<sup>17</sup>

**D. Spectral Diffusion in Small Reverse Micelles.** To quantify the changes in the 2D spectra, and to extract the FFCFs for small reverse micelles, the CLS was calculated for a  $\pm 30 \text{ cm}^{-1}$  range around the 2D IR maximum location for  $w_0 = 2, 4$ , and 7.5. The CLS curves for these three AOT reverse micelles are shown in Figure 11. Orientational relaxation measurements for the  $w_0 = 2$  and 4 reverse micelles show that the structural dynamics behave essentially as a single ensemble. In the previous sections, we treated  $w_0 = 7.5$  approximately using the core-interface decomposition approach for the 2D IR spectral diffusion dynamics. Here  $w_0 = 7.5$  was treated in the same manner as  $w_0 = 2$  and 4 for comparison. The experimental  $T_w$  range is limited by the vibrational lifetimes of each sample. Thus, data cannot be taken at the same  $T_w$  values for each sample (see Figure 11).

The general trend of the CLS data is that spectral diffusion slows down as the water pool size decreases. The CLS curves, in conjunction with the IR spectra of the samples, can be used to extract the FFCF parameters.<sup>39,40</sup> The FFCF parameters determined for reverse micelles  $w_0 = 2, 4$ , and 7.5 are listed in Table 6. The FFCF for a small reverse micelle takes the form of a biexponential decay with a static offset and a motionally narrowed (homogeneous) component. All three FFCFs have a fast time constant of  $\sim 1$  ps, and a slower time constant of  $\sim 6$ –10 ps. Bulk water has a fast time constant of  $\sim 400$  fs, which is attributed to fast, very local hydrogen bond fluctuations.<sup>27,28</sup> Given the similarity in time scales and that the small reverse micelles represent very constrained environments, it is reasonable to conclude that the  $\sim 1$  ps time scale is also due to local hydrogen bond fluctuations.

It is useful to note that neither treatment of the  $w_0 = 7.5$  reverse micelle is truly correct. In this section,  $w_0 = 7.5$  is treated as a single ensemble in the same way as  $w_0 = 2$  and 4. However, in contrast to  $w_0 = 2$  and 4 for which the orientational relaxation does not separate into interfacial and core components,  $w_0 = 7.5$  does separate into two components. In the previous section, the CLS data were decomposed to obtain the interfacial component. The two-component CLS procedure requires that the spectral diffusion is known for the core. Bulk water was used to model the core, but the orientational relaxation data show that the core is not bulk-like in AOT  $w_0 = 7.5$ . Therefore, there are uncertainties associated with each model for AOT  $w_0 = 7.5$ .

The static offset in the FFCF (not present in bulk water) arises from the extremely slow motions of the water molecules in the small reverse micelles. For spectral diffusion to be complete in any system, all water molecules must experience all environments. Diffusion through the reverse micelles or exchange of populations between an OD hydroxyl bound to the interface and one bound to another water oxygen will occur very slowly in the highly confined environments of the smallest reverse micelles. It is likely that slow diffusion and exchange contribute to the static offset.

The slowest time scale for bulk water spectral diffusion is 1.7 ps, corresponding to global hydrogen bond reorganization.<sup>26</sup> It is possible that the intermediate time scale decay of the FFCF, 6–10 ps, is caused by hydrogen bond rearrangement of water molecules bound to the waters directly at the interface with ones that have at least one or possibly both hydroxyls not bound to the interface. For the large reverse micelles, this mechanism was proposed because of the similarity of times for the interfacial and bulk water spectral diffusion. For the small reverse micelles, the dynamics will be slower and as the water nanopool becomes smaller, the dynamics will become increasingly slow. Another possibility that was suggested previously is that interfacial topography roughness contributes to the inhomogeneous broadening and, by extension, motions of the surfactant head groups will cause spectral diffusion.<sup>24</sup>

In addition to the time constants, the FFCF also contains frequency fluctuation amplitudes ( $\Delta$  terms) and a motionally narrowed component. Each time scale, including the static offset, produces a significant amount of inhomogeneous broadening. The motionally narrowed component ( $\Gamma$ ) is roughly the same for  $w_0 = 2$  and 4, but is significantly greater for  $w_0 = 7.5$ . Again, it needs to be noted that  $w_0 = 7.5$  is not strictly a small reverse micelle.

#### IV. CONCLUDING REMARKS

Spectral diffusion was measured for water inside of a range of AOT reverse micelles from  $w_0 = 16.5$  (5.8 nm diameter) through  $w_0 = 2$  (1.7 nm diameter) using 2D IR vibrational echo spectroscopy. We observe that the process of spectral diffusion, described by the FFCF, undergoes significant changes as the water pool size inside the reverse micelles increases. The 2D IR spectra for large reverse micelles ( $w_0 = 12$  and 16.5) are a combination of signals from a bulk water core and a shell of interfacial waters at the surfactant head groups. Each of these ensembles has its own FFCF. Because the FFCF for bulk water is known, the FFCF for the interfacial region can be calculated from known data and other experimentally measured parameters. It is important to note that a CLS curve calculated on the actual experimental 2D spectra does not yield a weighted average of the FFCFs and that in order for meaningful information to be obtained, the CLS for large reverse micelles must be decomposed into bulk and interfacial contributions.

The similarity between the FFCFs for AOT  $w_0 = 12$  and 16.5 further corroborates previous conclusions that the dynamics at the interface are virtually the same for all AOT large reverse micelles.<sup>6,8,9</sup> For the large reverse micelles, a component of the interfacial spectral diffusion is very similar to that of bulk water, which corresponds to hydrogen bond network randomization. It was postulated that the  $\sim 1.6$  ps component of the interfacial spectral diffusion is associated with hydrogen bond rearrangement of core water molecules that are interacting with the interfacial water molecules. Spectral diffusion was also compared for large Igepal and AOT reverse micelles of diameter 5.8 nm (Igepal  $w_0 = 12$  and AOT  $w_0 = 16.5$ ). The results suggest that dynamics that give rise to spectral diffusion are not affected much by the chemical nature of the interface. This was found to be true for orientational relaxation as well.<sup>17</sup> The interfacial dynamic processes in large reverse micelles are mainly determined by the presence of an interface rather than its chemical nature.

The  $w_0 = 7.5$  system was also treated as a large reverse micelle because, based on orientational relaxation experiments, the

$w_0 = 7.5$  water pool can be divided into core and interfacial regions. However, the core region is not the same as bulk water. The actual core region for  $w_0 = 7.5$  cannot be measured separately, so bulk water was used as an approximation in the decomposition of the spectral diffusion dynamics to obtain the interfacial FFCF. It is found that the interfacial FFCF for  $w_0 = 7.5$  is slower than the interfacial FFCFs for  $w_0 = 12$  and 16.5, which are about the same. We have presented two sets of FFCF results for AOT  $w_0 = 7.5$ , treating it as both a large and a small reverse micelle. Neither is precisely correct, but the results permit comparisons to the larger and smaller reverse micelles.

In small reverse micelles ( $w_0 = 2$  and 4), the FFCF takes the form of a biexponential decay plus an offset and a homogeneous component. A fast decay of  $\sim 1$  ps is attributed to local hydrogen bond fluctuations (present in bulk water), but the slower  $\sim 6-10$  ps decay represents processes that are not present in bulk water, such as surface topography fluctuations of the interface or slow hydrogen bond rearrangement of water molecules bound to interfacial water molecules. The static offset also has no analogue in bulk water and is associated with very slow processes such as diffusion to the interface and exchange between hydroxyls bound to the interface and ones that are not.

MD simulations have been used to study the orientational relaxation of water in AOT reverse micelles.<sup>31,32,61</sup> In light of the new extended two component CLS method, it would be very interesting to explore the spectral diffusion dynamics of interfacial water molecules in large reverse micelles using MD simulations.

## AUTHOR INFORMATION

### Corresponding Author

\*E-mail: fayer@stanford.edu. Phone: (650) 723-4446. Fax: (650) 723-4817.

## ACKNOWLEDGMENT

We would like to thank the Department of Energy (DE-FG03-84ER13251) for support of this research. D.B.W. thanks the Stanford Graduate Fellowship program for a fellowship.

## REFERENCES

- (1) Laage, D.; Hynes, J. T. *Science* **2006**, *311*, 832.
- (2) Laage, D.; Hynes, J. T. *J. Phys. Chem. B* **2008**, *112*, 14230.
- (3) Bakker, H. J.; Kropman, M. F.; Omata, Y.; Woutersen, S. *Phys. Scr.* **2004**, *69*, C14.
- (4) Laage, D.; Stirnemann, G.; Hynes, J. T. *J. Phys. Chem. B* **2009**, *113*, 2428.
- (5) Fenn, E. E.; Moilanen, D. E.; Levinger, N. E.; Fayer, M. D. *J. Am. Chem. Soc.* **2009**, *131*, 5530.
- (6) Moilanen, D. E.; Fenn, E. E.; Wong, D.; Fayer, M. D. *J. Chem. Phys.* **2009**, *131*, 014704.
- (7) Moilanen, D. E.; Wong, D.; Rosenfeld, D. E.; Fenn, E. E.; Fayer, M. D. *Proc. Natl. Acad. Sci. U.S.A.* **2009**, *106*, 375.
- (8) Moilanen, D. E.; Fenn, E. E.; Wong, D.; Fayer, M. D. *J. Phys. Chem. B* **2009**, *113*, 8560.
- (9) Moilanen, D. E.; Fenn, E. E.; Wong, D.; Fayer, M. D. *J. Am. Chem. Soc.* **2009**, *131*, 8318.
- (10) Piletic, I. R.; Moilanen, D. E.; Spry, D. B.; Levinger, N. E.; Fayer, M. D. *J. Phys. Chem. A* **2006**, *110*, 4985.
- (11) Cringus, D.; Bakulin, A.; Lindner, J.; Vohringer, P.; Pshenichnikov, M. S.; Wiersma, D. A. *J. Phys. Chem. B* **2007**, *111*, 14193.
- (12) Cringus, D.; Lindner, J.; Milder, M. T. W.; Pshenichnikov, M. S.; Vohringer, P.; Wiersma, D. A. *Chem. Phys. Lett.* **2005**, *408*, 162.
- (13) Dokter, A. M.; Woutersen, S.; Bakker, H. J. *Phys. Rev. Lett.* **2005**, *94*, 178301.
- (14) Dokter, A. M.; Woutersen, S.; Bakker, H. J. *Proc. Natl. Acad. Sci. U.S.A.* **2006**, *103*, 15355.
- (15) Piletic, I.; Tan, H.-S.; Moilanen, D. E.; Spry, D. B.; Fayer, M. D. Vibrational Echo and Pump–Probe Spectroscopic Studies of the Dynamics of Water Molecules Confined to Nanoscopic Dimensions. In *Femtochemistry VII: Fundamental Ultrafast Processes in Chemistry, Physics, and Biology*; Castleman, A. W., Kimble, M. L., Eds.; Elsevier: Amsterdam, 2006; pp 195.
- (16) Piletic, I. R.; Tan, H.-S.; Fayer, M. D. *J. Phys. Chem. B* **2005**, *109*, 21273.
- (17) Fenn, E. E.; Wong, D. B.; Fayer, M. D. *Proc. Natl. Acad. Sci. U.S.A.* **2009**, *106*, 15243.
- (18) Moilanen, D. E.; Levinger, N.; Spry, D. B.; Fayer, M. D. *J. Am. Chem. Soc.* **2007**, *129*, 14311.
- (19) Tan, H.-S.; Piletic, I. R.; Fayer, M. D. *J. Chem. Phys.* **2005**, *122*, 174501(9).
- (20) Tan, H.-S.; Piletic, I. R.; Fayer, M. D. *J. Opt. Soc. Am. B: Opt. Phys.* **2005**, *22*, 2009.
- (21) Zulauf, M.; Eicke, H. F. *J. Phys. Chem.* **1979**, *83*, 480.
- (22) Kinugasa, T.; Kondo, A.; Nishimura, S.; Miyachi, Y.; Nishii, Y.; Watanabe, K.; Takeuchi, H. *Colloids Surf., A: Physicochem. Eng. Aspects* **2002**, *204*, 193.
- (23) Eicke, H.-F.; Rehak, J. *Helv. Chim. Acta* **1976**, *59*, 2883.
- (24) Fenn, E. E.; Wong, D. B.; Fayer, M. D. *J. Chem. Phys.* **2011**, *134*, 054512.
- (25) Mukamel, S. *Principles of Nonlinear Optical Spectroscopy*; Oxford University Press: New York, 1995.
- (26) Park, S.; Fayer, M. D. *Proc. Natl. Acad. Sci. U.S.A.* **2007**, *104*, 16731.
- (27) Lawrence, C. P.; Skinner, J. L. *J. Chem. Phys.* **2003**, *118*, 264.
- (28) Corcelli, S. A.; Lawrence, C. P.; Asbury, J. B.; Steinel, T.; Fayer, M. D.; Skinner, J. L. *J. Chem. Phys.* **2004**, *121*, 8897.
- (29) Izquierdo, C.; Moya, M. L.; Usero, J. L.; Casado, J. *Monatsh. Chem.* **1992**, *123*, 383.
- (30) Tan, H.-S.; Piletic, I. R.; Riter, R. E.; Levinger, N. E.; Fayer, M. D. *Phys. Rev. Lett.* **2005**, *94*, 057405.
- (31) Pieniazek, P. A.; Lin, Y.-S.; Chowdhary, J.; Ladanyi, B. M.; Skinner, J. L. *J. Phys. Chem. B* **2009**, *113*, 15017.
- (32) Abel, S.; Sterpone, F.; Bandyopadhyay, S.; Marchi, M. *J. Phys. Chem. B* **2004**, *108*, 19458.
- (33) Freda, M.; Onori, G.; Paciaroni, A.; Santucci, A. *Chem. Phys. Lett.* **2001**, *348*, 311.
- (34) Lipgens, S.; Schubel, D.; Schlicht, L.; Spilgues, J.-H.; Ilgenfritz, G.; Eastoe, J.; Heenan, R. K. *Langmuir* **1998**, *14*, 1041.
- (35) Gaffney, K. J.; Piletic, I. R.; Fayer, M. D. *J. Chem. Phys.* **2003**, *118*, 2270.
- (36) Woutersen, S.; Bakker, H. J. *Nature (London)* **1999**, *402*, 507.
- (37) Corcelli, S.; Lawrence, C. P.; Skinner, J. L. *J. Chem. Phys.* **2004**, *120*, 8107.
- (38) Park, S.; Kwak, K.; Fayer, M. D. *Laser Phys. Lett.* **2007**, *4*, 704.
- (39) Kwak, K.; Park, S.; Finkelstein, I. J.; Fayer, M. D. *J. Chem. Phys.* **2007**, *127*, 124503.
- (40) Kwak, K.; Rosenfeld, D. E.; Fayer, M. D. *J. Chem. Phys.* **2008**, *128*, 204505.
- (41) Schmidt, J. R.; Corcelli, S. A.; Skinner, J. L. *J. Chem. Phys.* **2005**, *123*, 044513(13).
- (42) Schmidt, J. R.; Roberts, S. T.; Loparo, J. J.; Tokmakoff, A.; Fayer, M. D.; Skinner, J. L. *J. Chem. Phys.* **2007**, *341*, 143.
- (43) Asbury, J. B.; Steinel, T.; Kwak, K.; Corcelli, S. A.; Lawrence, C. P.; Skinner, J. L.; Fayer, M. D. *J. Chem. Phys.* **2004**, *121*, 12431.
- (44) Asbury, J. B.; Steinel, T.; Stromberg, C.; Corcelli, S. A.; Lawrence, C. P.; Skinner, J. L.; Fayer, M. D. *J. Phys. Chem. A* **2004**, *108*, 1107.
- (45) Gruenbaum, S. M.; Skinner, J. L. *J. Chem. Phys.* **2011**, *135*, 075101.
- (46) Lin, Y. S.; Pieniazek, P. A.; Yang, M.; Skinner, J. L. *J. Chem. Phys.* **2010**, *132*, 174505.
- (47) Kenkre, V. M.; Tokmakoff, A.; Fayer, M. D. *J. Chem. Phys.* **1994**, *101*, 10618.

- (48) Egorov, S. A.; Berne, B. J. *J. Chem. Phys.* **1997**, *107*, 6050.  
(49) Steinel, T.; Asbury, J. B.; Zheng, J. R.; Fayer, M. D. *J. Phys. Chem. A* **2004**, *108*, 10957.  
(50) Woutersen, S.; Emmerichs, U.; Bakker, H. J. *J. Chem. Phys.* **1997**, *107*, 1483.  
(51) Gaffney, K.; Piletic, I. R.; Fayer, M. D. *J. Phys. Chem. A* **2002**, *106*, 9428.  
(52) Gaffney, K. J.; Davis, P. H.; Piletic, I. R.; Levinger, N. E.; Fayer, M. D. *J. Phys. Chem. A* **2002**, *106*, 12012.  
(53) Loparo, J. J.; Fecko, C. J.; Eaves, J. D.; Roberts, S. T.; Tokmakoff, A. *Phys. Rev. B* **2004**, *70*, 180201.  
(54) Rezus, Y. L. A.; Bakker, H. J. *J. Chem. Phys.* **2005**, *123*, 114502.  
(55) Lipari, G.; Szabo, A. *J. Am. Chem. Soc.* **1982**, *104*, 4546.  
(56) Fenn, E. E.; Fayer, M. D. *J. Chem. Phys.* **2011**, *135*, 074502.  
(57) Smith, J. D.; Saykally, R. J.; Geissler, P. L. *J. Am. Chem. Soc.* **2007**, *129*, 13847.  
(58) Ebbinghaus, S.; Kim, S. J.; Heyden, M.; Yu, X.; Heugen, U.; Gruebele, M.; Leitner, D. M.; Havenith, M. *Proc. Natl. Acad. Sci. U.S.A.* **2007**, *104*, 20749.  
(59) Makarov, V. A.; Feig, M.; Andrews, B. K.; Pettitt, B. M. *Biophys. J.* **1998**, *75*, 150.  
(60) Leitner, D. M.; Havenith, M.; Gruebele, M. *Int. Rev. Phys. Chem.* **2006**, *25*, 553.  
(61) Faeder, J.; Ladanyi, B. M. *J. Phys. Chem. B* **2000**, *104*, 1033.